Journal of Power Sources 189 (2009) 114–120

Contents lists available at ScienceDirect

Journal of Power Sources

journal homepage: www.elsevier.com/locate/jpowsour

Improvement of cathode performance of $LiMn_2O_4$ as a cathode active material for Li ion battery by step-by-step supersonic-wave treatments

Naoto Kitamura, Hidenobu Iwatsuki, Yasushi Idemoto*

Department of Pure and Applied Chemistry, Faculty of Science and Technology, Tokyo University of Science, 2641 Yamazaki, Noda, Chiba 278-8510, Japan

ARTICLE INFO

Article history:
Received 24 July 2008
Received in revised form 4 October 2008
Accepted 10 October 2008
Available online 21 October 2008

Keywords:
Lithium ion battery
Cathode
Supersonic wave
Spinel structure

ABSTRACT

As a novel partial substitution and surface modification process, we focused on a step-by-step (double-step) supersonic-wave treatment in a Zn-containing aqueous solution without any heat-treatments, and performed the treatment on $LiMn_2O_4$ powder. From XRD measurements, it was demonstrated that the lattice constant of $LiMn_2O_4$ decreased slightly by the treatments, indicating a partial substitution of Zn for Mn. It was also suggested by SEM–EDX and XPS that Zn was well dispersed in/on the samples and their surfaces were modified by Zn compounds. Such a partial substitution and surface modification was supported by crystal structure analysis based on the Rietveld method using neutron diffraction. Cycle performance of $LiMn_2O_4$ was significantly improved by the step-by-step supersonic-wave treatments. In the processes, it was especially effective for the improvement to apply lower and higher frequencies at the first and second steps, respectively, keeping the power higher. The cathode property improvement was considered due to the partial substitution and the surface coating caused by the step-by-step supersonic-wave treatments. From the investigation on the cathodes and electrolytes after the cycle tests, it was suggested that the crystal structure of $LiMn_2O_4$ was stabilized by the treatments.

1. Introduction

Recently, $LiMn_2O_4$ with the spinel structure has attracted much attention as a cathode material for Li ion battery, due to its lower cost and lower toxicity than commercialized $LiCoO_2$-based materials. Due to dissolution of Mn into liquid electrolyte etc., however, the capacity decreases significantly during charge–discharge cycles [1–7]. Partial substitution of another metal for Mn is one of the most effective methods to suppress such a capacity fade in $LiMn_2O_4$ [7–20]. For example, our previous work clarified that $LiMn_{2-x}M_xO_4$ (M = Al, Mg, Cr, Co, Ni and Zn) exhibited higher thermodynamic and structural stabilities compared with $LiMn_2O_4$, and the stabilities resulted in better cathode performances [3,14,16–20]. In addition, some investigations demonstrated that surface coating with oxides was also effective to improve the cycle performance of $LiMn_2O_4$ [21–28]. From such background, as partial substitution and/or surface coating methods, we have recently focused on a supersonic-wave treatment, and found that a cathode performance of $LiMn_2O_4$ became better by heat-treating the material at 600 °C after supersonic-wave treatment (e.g. 28 kHz of the frequency) in a Zn-containing aqueous solution [29].

In order to realize comparable improvement without the heat-treatment, i.e. only with "soft processes", we applied "a step-by-step supersonic-wave treatment" for $LiMn_2O_4$ in this work. In the treatment, we performed a supersonic-wave treatment with lower frequency and then with higher frequency on $LiMn_2O_4$ powder in a Zn-containing aqueous solution. The obtained powder was characterized with X-ray diffraction measurement, chemical composition and Mn valence analyses, and the cathode properties were investigated with CV measurements and charge–discharge cycle tests. We also performed the Rietveld analysis using neutron diffraction pattern for the purpose of crystal structure analysis. Based on these results, we discussed how the step-by-step supersonic-wave treatment affected on the $LiMn_2O_4$ powder and thus the cathode performance.

2. Experimental

$LiMn_2O_4$ was synthesized with the solid-state reaction using Li_2CO_3 (99.9%, Wako Pure Chemical Industries, Ltd.) and MnO_2 (99.5%, Wako Pure Chemical Industries, Ltd.) as starting materials. The mixture was heat-treated at 700 °C for 24 h in air. A supersonic-wave treatment with a frequency of 28 or 40 kHz and the power of 150 or 300 W was applied to the obtained $LiMn_2O_4$ powder in a Zn-containing aqueous solution which was prepared by dissolving zinc acetate (99.9%, Wako Pure Chemical Industries, Ltd.) into dis-

* Corresponding author. Tel.: +81 4 7122 9493; fax: +81 4 7125 7761.
E-mail address: idemoto@rs.noda.tus.ac.jp (Y. Idemoto).

0378-7753/$ – see front matter © 2008 Elsevier B.V. All rights reserved.
doi:10.1016/j.jpowsour.2008.10.046

Table 1
Lattice constants and full-width of half-maximums (1 1 1) of the samples after step-by-step supersonic-wave treatments in an aqueous solution containing Zn. Those of $LiMn_2O_4$ before the treatments are also listed as a reference.

Sample	a/nm	FWHM (1 1 1)
$LiMn_2O_4$	0.8242(1)	0.1574
28 kHz (150 W)–200 kHz (300 W)	0.8229(1)	0.1181
28 kHz (150 W)–950 kHz (300 W)	0.8231(2)	0.0984
40 kHz (150 W)–200 kHz (300 W)	0.8226(1)	0.1181
28 kHz (300 W)–200 kHz (300 W)	0.8238(2)	0.1181
28 kHz (300 W)–950 kHz (300 W)	0.8238(2)	0.1181

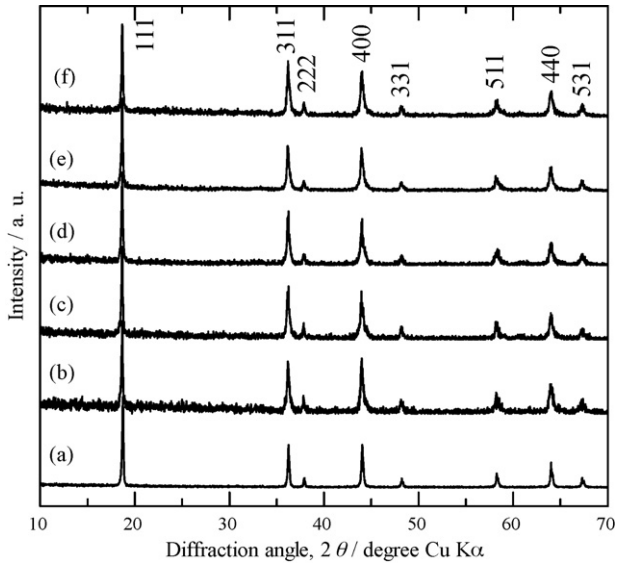

Fig. 1. Powder X-ray diffraction patterns of the samples after step-by-step supersonic-wave treatments in an aqueous solution containing Zn. That of $LiMn_2O_4$ before the treatments is also shown as a reference. (a) $LiMn_2O_4$, (b) 28 kHz (150 W)–200 kHz (300 W), (c) 28 kHz (150 W)–950 kHz (300 W), (d) 40 kHz (150 W)–200 kHz (300 W), (e) 28 kHz (300 W)–200 kHz (300 W) and (f) 28 kHz (300 W)–950 kHz (300 W).

tilled water. Taking our previous work into account [29], the weight ratio of zinc acetate to distilled water was fixed as 4:96 in this work. Subsequently, a supersonic-wave treatment with higher frequency (200 or 950 kHz) and the power of 300 W were performed in the solution. Both first- and second-step treatments were carried out at room temperature for 10 min. The products were dried at 100 °C for 24 h. In this manuscript, for example, a step-by-step supersonic-wave treatment where 28 kHz of a frequency with a power of 150 W as a first step and 200 kHz of a frequency with a power of 300 W as a second step were applied, was represented as "28 kHz (150 W)–200 kHz (300 W)".

Phase identification and determination of lattice constants of the obtained materials were performed with X-ray diffraction measurements (Philips, X'Pert Pro), and their chemical compositions and Mn valences were evaluated with inductively coupled plasma, ICP (Shimadzu Co., ICPS-7500) and iodimetry [3]. Morphologies of the powders were observed by scanning electron microscope, SEM (Hitachi, S-2600N) with energy dispersive X-ray spectroscopy, EDX, system. Their surface compositions were studied by X-ray photoelectron spectroscopy, XPS (Shimadzu Co.,

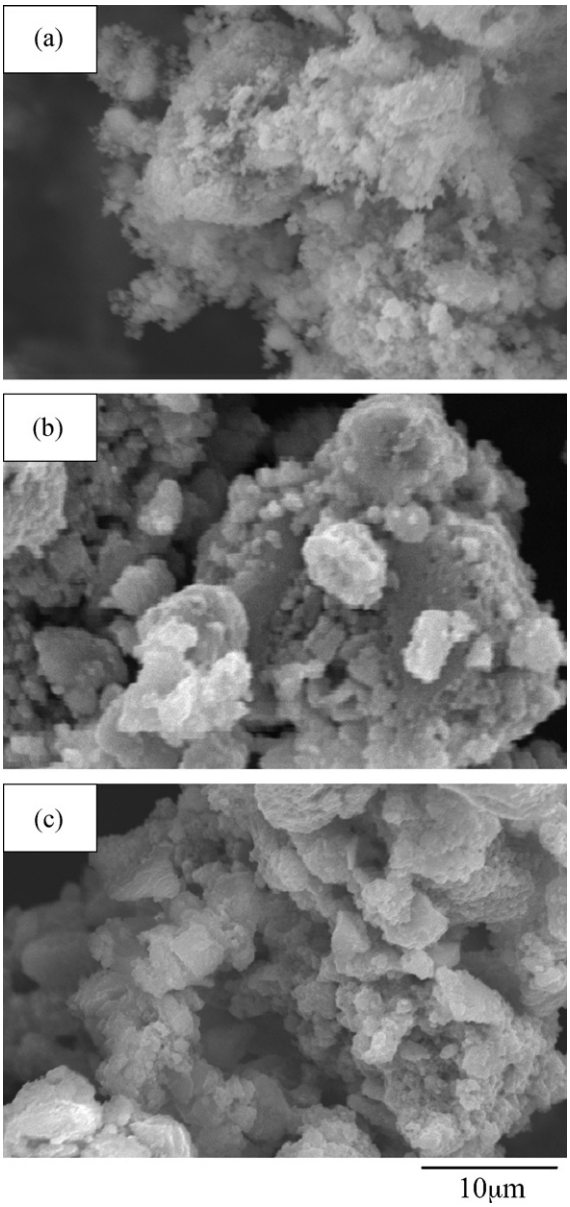

Fig. 2. SEM photographs of the samples after step-by-step supersonic-wave treatments in an aqueous solution containing Zn. That of $LiMn_2O_4$ before the treatments is also shown as a reference. (a) $LiMn_2O_4$, (b) 28 kHz (150 W)–200 kHz (300 W) and (c) 28 kHz (300 W)–200 kHz (300 W).

Table 2
Compositions, Mn valences and oxygen contents of the samples after step-by-step supersonic-wave treatments in an aqueous solution containing Zn. Those of $LiMn_2O_4$ before the treatments are also listed as a reference.

Sample	Li	Mn	Zn	Mn valence	Oxygen content
$LiMn_2O_4$	1.025(3)	1.974(3)		3.521(1)	3.988
28 kHz (150 W)–200 kHz (300 W)	1.107(3)	1.804(3)	0.0878(1)	3.554(2)	3.847
28 kHz (150 W)–950 kHz (300 W)	1.127(1)	1.786(2)	0.0862(1)	3.551(1)	3.820
40 kHz (150 W)–200 kHz (300 W)	1.109(3)	1.802(3)	0.0875(4)	3.559(3)	3.848
28 kHz (300 W)–200 kHz (300 W)	1.059(2)	1.853(2)	0.0873(1)	3.588(1)	3.941
28 kHz (300 W)–950 kHz (300 W)	1.068(1)	1.844(1)	0.0880(1)	3.572(1)	3.914

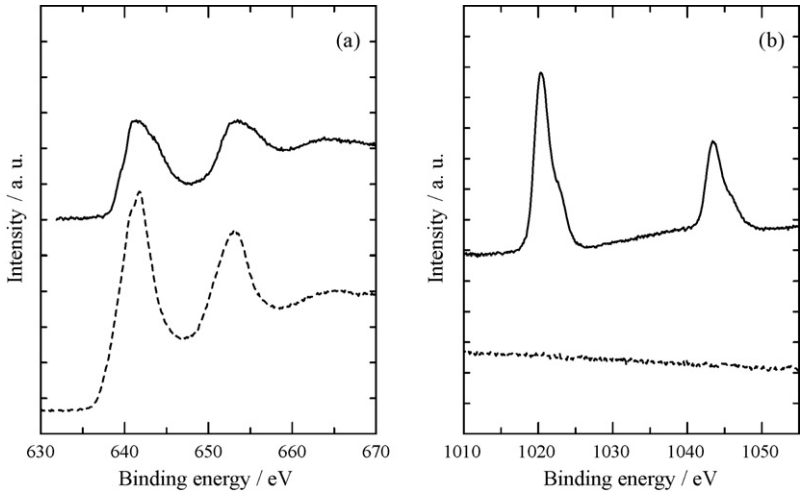

Fig. 3. XPS spectra of (a) Mn 2p and (b) Zn 2p orbitals of $LiMn_2O_4$ (a broken line) and the sample after a step-by-step supersonic-wave treatment (a solid line). The treatment condition is represented as "28 kHz (300 W)–200 kHz (300 W)".

AXIS-HI) using Mg Kα line. In order to investigate the crystal structure in detail, we also measured a neutron diffraction pattern with HERMES [30] of IMR at JRR-3M in JAERI. The pattern was analyzed based on the Rietveld technique using Rietan-2000 program [31]. Electrochemical properties of the samples after the step-by-step supersonic-wave treatments were investigated at room temperature with the charge–discharge cycle tests (Hokuto Denko Co., HJR-110 m SM6) and CV measurements (Hokuto Denko Co., HZ-3000). The cell for these measurements was a conventional three-electrode cell. The working electrode was prepared by mixing the active material, acetylene black, PTFE with a weight ratio of 5:2:2. As the reference and counter electrodes, Li foil was utilized. The electrolyte was a 1.0 M $LiClO_4$ solution where the solvent was prepared by mixing PC and DMC in the same volume. The CV measurements were performed with a scan speed of 0.1 mV s^{-1} and a scan range of 3.5–4.3 V vs. Li/Li^+. The charge–discharge cycle tests were carried out with a current density of 0.2 mA cm^{-2} in the voltage from 3.5 to 4.3 V vs. Li/Li^+. After the measurements, we studied again their crystal structures with XRD and Mn dissolution amount into the electrolyte with ICP.

3. Results and discussion

3.1. Characterization

Fig. 1 shows powder XRD patterns of samples after step-by-step supersonic-wave treatments. That of $LiMn_2O_4$ before the treatments is also given as a reference. From this figure, it was confirmed that all the diffraction peaks of the samples after the treatments could be attributable to the spinel structure (S.G.; $Fd-3m$). Lattice constants calculated from the patterns and full-width of half-maximums (FWHMs) of the diffraction peak (1 1 1) are listed in Table 1. The lattice constant and the full-width of half-maximums became slightly smaller by the step-by-step supersonic-wave treatments regardless of the treatment conditions. Table 2 presents their metal compositions, Mn valences and oxygen contents determined by ICP and iodimetry. The total metal compositions were assumed to be 3. After the supersonic-wave treatments, we could detect Zn as a component, and the content was almost independent of the treatment conditions. It was also demonstrated that Mn valence was increased by the supersonic-wave treatments. Such an increase of Mn valence suggests that a part of Zn^{2+} substitute for $Mn^{3+/4+}$ after the step-by-step supersonic-wave treatments. Considering this, the decreases of the lattice constants by the treatments shown in Table 1 may reflect a difference of the ionic radii between Mn^{3+} and Mn^{4+}. In order to investigate particle sizes and Zn distributions, SEM and EDX measurements were carried out. Part of the results was shown in Fig. 2. By comparing the results for the samples before and after the step-by-step supersonic-wave treatments, it was found that the particle sizes were not affected by the treatments. It was also confirmed with EDX that Zn was well dispersed in/on the materials without compositional segregation. In order to clarify a surface metal composition of the sample after the step-by-step supersonic-wave treatment, XPS measurements were also performed. Fig. 3 shows XPS spectra of $LiMn_2O_4$ before and after a supersonic-wave treatment represented as 28 kHz (300 W)–200 kHz (300 W). After the treatments, peaks attributable to 2p orbitals of Zn were observed in the sample and those of Mn were considerably reduced. Taking it into account that an XPS measurement is a nano-scale surface analysis, this result suggests that the step-by-step supersonic-wave treatment caused surface coating of $LiMn_2O_4$ particle with Zn compounds in addition to the partial substitution mentioned above.

3.2. Cathode performance

As for samples after the step-by-step supersonic-wave treatments, we studied their cathode properties by CV measurements and charge–discharge cycle tests. Figs. 4 and 5 show the results for samples after the treatments represented as 28 kHz (150 W)–200 kHz (300 W) and 28 kHz (300 W)–200 kHz (300 W). In these figures, the results for $LiMn_2O_4$ before the treatments are also presented. From the CVs in Fig. 4, it was clarified that the samples exhibited redox reactions at the 4 V region even after the supersonic-wave treatments although their current densities decreased. In the case of $LiMn_2O_4$ before the treatments, both the cathodic and anodic processes had two distinct peaks, i.e. two distinct redox reactions. As for the samples after the step-by-step supersonic-wave treatments, however, such a distinction between two redox reactions in both the processes became ambiguous. Such a tendency was also observed in their charge and discharge curves given in Fig. 5. In addition to this, the charge–discharge cycle tests demonstrated that the cycle performance was improved drastically by the step-by-step supersonic-wave treatments although the first capacity was deteriorated. These changes in the charge–discharge curves caused by the treatments were considerably similar to those

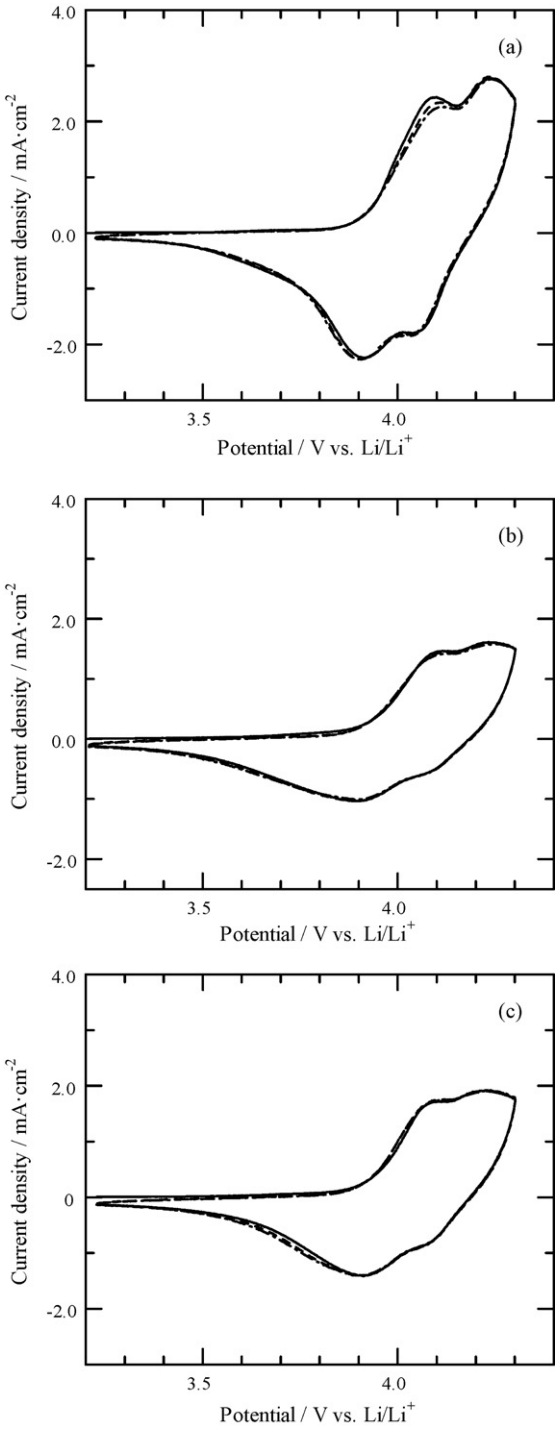

Fig. 4. Cyclic voltammograms of the samples after step-by-step supersonic-wave treatments in an aqueous solution containing Zn. That of $LiMn_2O_4$ before the treatments is also shown as a reference. (a) $LiMn_2O_4$, (b) 28 kHz (150 W)–200 kHz (300 W) and (c) 28 kHz (300 W)–200 kHz (300 W) (–, 1st cycle; ——, 2nd cycle; –·–, 3rd cycle).

observed in $LiMn_{2-x}Zn_xO_4$ prepared by a conventional solid-state reaction [17–19].

In order to clarify an effect of the Zn-containing aqueous solution in the treatment process, we performed step-by-step supersonic-wave treatments with and without a Zn aqueous solution. Cycle performances of samples after the treatments are shown in Fig. 6, and their first and 50th discharge capacities and capacity maintenances are listed in Table 3. Results of $LiMn_2O_4$ before the

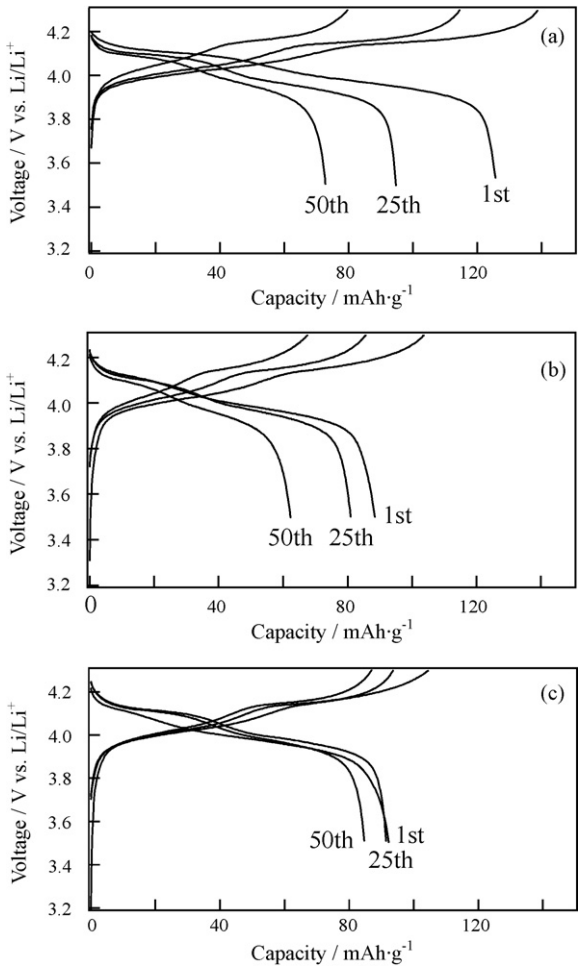

Fig. 5. Charge–discharge curves of the samples after step-by-step supersonic-wave treatments in an aqueous solution containing Zn. That of $LiMn_2O_4$ before the treatments is also shown as a reference. (a) $LiMn_2O_4$, (b) 28 kHz (150 W)–200 kHz (300 W) and (c) 28 kHz (300 W)–200 kHz (300 W).

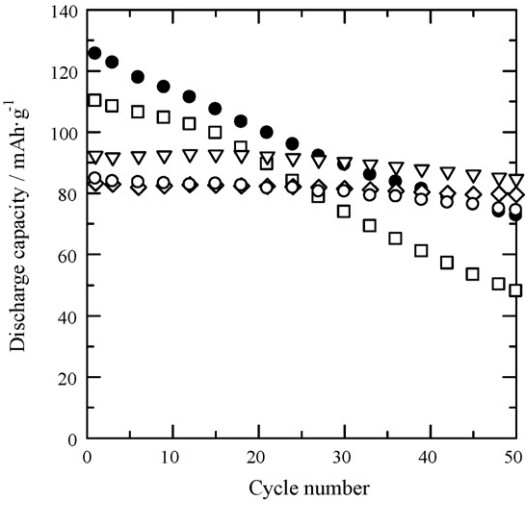

Fig. 6. Cycle performances of the samples after various treatments at 25 °C with a current density of 0.2 mA cm^{-2}. That of $LiMn_2O_4$ before the treatments is also shown as a reference. ●: $LiMn_2O_4$; ▽: 28 kHz (300 W)–200 kHz (300 W); □: 28 kHz (300 W)–200 kHz (300 W) in pure water; ○: 28 kHz and heat-treatment (600 °C); ◇: immersion in Zn-containing aqueous solution (without supersonic-wave treatment).

Table 3
Discharge capacities of the samples after various treatments at 25 °C with a current density of 0.2 mA cm^{-2}. That of $LiMn_2O_4$ before the treatments is also listed as a reference.

Sample	First discharge capacity/mAh g^{-1}	50th discharge capacity/mAh g^{-1}	Capacity maintenance/%
$LiMn_2O_4$	125.6	72.7	57.9
28 kHz (300 W)–200 kHz (300 W)	92.2	84.7	91.7
28 kHz (300 W)–200 kHz (300 W) in H_2O	110.2	48.1	43.6
28 kHz and a heating at 600 °C[a]	84.8	74.4	87.7
Immersion in Zn aqueous solution	83.2	79.5	95.5

[a] This result was reported in our previous work [29].

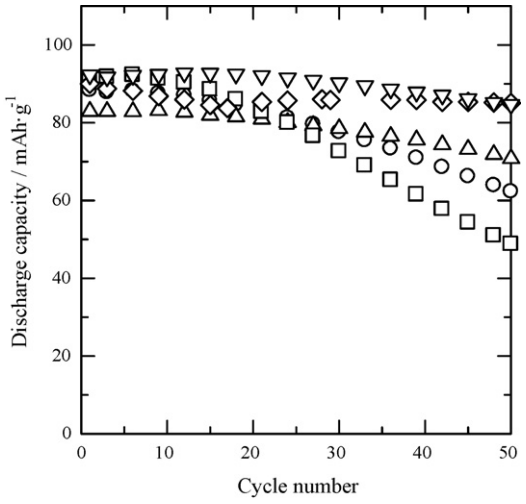

Fig. 7. Cycle performances of the samples after step-by-step supersonic-wave treatments in an aqueous solution containing Zn. These data were measured at 25 °C with a current density of 0.2 mA cm^{-2}. ○: 28 kHz (150 W)–200 kHz (300 W); △: 28 kHz (150 W)–950 kHz (300 W); □: 40 kHz (150 W)–200 kHz (300 W); ▽: 28 kHz (300 W)–200 kHz (300 W); ◇: 28 kHz (300 W)–950 kHz (300 W).

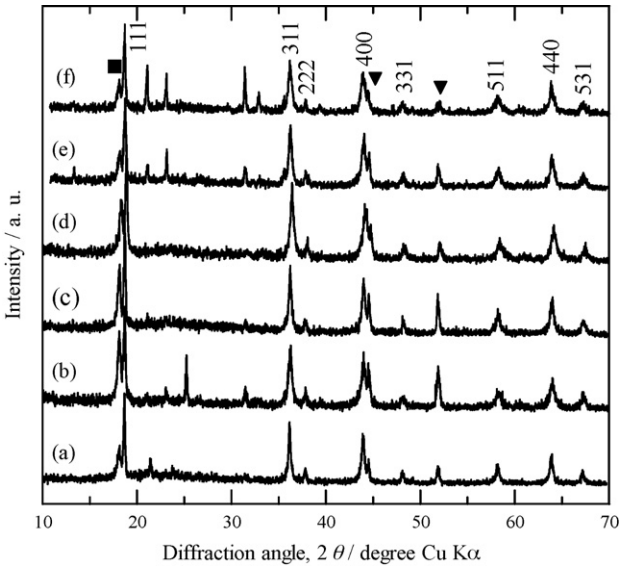

Fig. 8. Powder X-ray diffraction patterns of the cathodes after 50 cycles. (a) $LiMn_2O_4$, (b) 28 kHz (150 W)–200 kHz (300 W), (c) 28 kHz (150 W)–950 kHz (300 W), (d) 40 kHz (150 W)–200 kHz (300 W), (e) 28 kHz (300 W)–200 kHz (300 W) and (f) 28 kHz (300 W)–950 kHz (300 W) (■: PTFE; ▼: Ni).

treatments are also given in the figure and table. It was clarified that the cycle performance was not improved by the step-by-step supersonic-wave treatment without the Zn-containing aqueous solution. This suggests that Zn in/on the $LiMn_2O_4$ plays an important role on the cycle performance improvement. Fig. 6 and Table 3 also present results of sample after an immersion in the same Zn aqueous solution without the supersonic-wave treatment. Although the cycle performance was also improved in this case, the discharge capacity was lower compared with that of the samples after the step-by-step supersonic-wave treatment in the Zn aqueous solution. In our previous work, we investigated cycle performances of $LiMn_2O_4$ after single-step supersonic-wave treatments in the Zn-containing solution. In the case of the single-step supersonic-wave treatments, a heat-treatment at 600 °C was necessary for a cycle performance improvement [29]. The step-by-step supersonic-wave treatment, however, could improve the cathode property of $LiMn_2O_4$ without any heat-treatments, and the discharge capacity and the capacity maintenance were comparable to those of the samples after the single-step supersonic-wave treatments accompanied by the heat-treatment, as shown in Fig. 6 and Table 3. Based on these results, it can be considered that a step-by-step supersonic-wave treatment in a Zn-containing aqueous solution is a promising soft process for a cathode property improvement.

Table 5
Ratios of full-width of half-maximums of the diffraction peaks (1 1 1) of the cathode active materials after the 50th discharge cycle to those before the cycle tests.

Sample	Ratio of FWHM (1 1 1)
$LiMn_2O_4$	2.00
28 kHz (150 W)–200 kHz (300 W)	1.33
28 kHz (150 W)–950 kHz (300 W)	1.60
40 kHz (150 W)–200 kHz (300 W)	1.00
28 kHz (300 W)–200 kHz (300 W)	1.00
28 kHz (300 W)–950 kHz (300 W)	1.00

Fig. 7 and Table 4 show cycle performances of samples after step-by-step supersonic-wave treatments with various frequencies and powers. From these results, it was found that lower and higher frequencies were effective in the first and second steps, respectively,

Table 4
Discharge capacities of the samples after step-by-step supersonic-wave treatments in an aqueous solution containing Zn. These data were measured at 25 °C with a current density of 0.2 mA cm^{-2}.

Sample	First discharge capacity/mAh g^{-1}	50th discharge capacity/mAh g^{-1}	Capacity maintenance/%
28 kHz (150 W)–200 kHz (300 W)	88.4	62.3	70.4
28 kHz (150 W)–950 kHz (300 W)	82.9	70.8	85.3
40 kHz (150 W)–200 kHz (300 W)	91.5	48.8	53.3
28 kHz (300 W)–200 kHz (300 W)	92.2	84.7	91.7
28 kHz (300 W)–950 kHz (300 W)	90.0	85.1	94.8

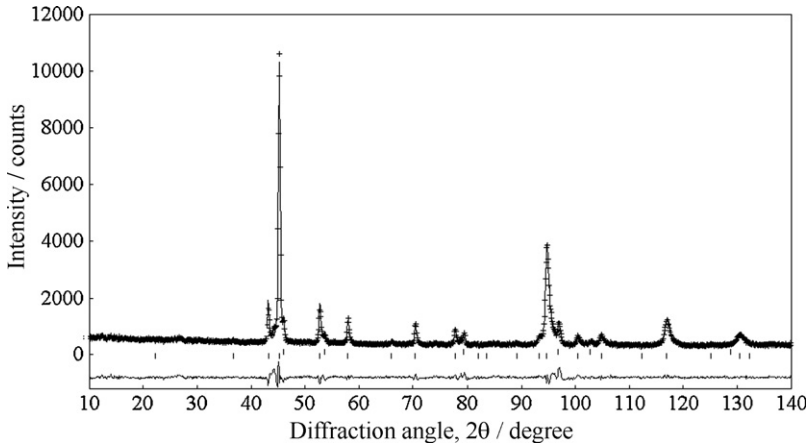

Fig. 9. Rietveld refinement patterns of the samples after the step-by-step supersonic-wave treatment [28 kHz (150 W)–950 kHz (300 W)]. Plus marks show observed neutron diffraction intensities, and a solid line represents calculated intensities. Vertical marks below the patterns indicate positions of allowed Bragg reflections (lower: $LiMn_{2-x}Zn_xO_4$; upper: Al from the apparatus). A curve at the bottom is a difference between the observed and calculated intensities in the same scale.

Table 6
Mn dissolution amount to the electrolyte after the 50th discharge cycle determined by ICP.

Sample	Mn dissolution amount
$LiMn_2O_4$	0.0593(1)
28 kHz (150 W)–200 kHz (300 W)	0.0611(1)
28 kHz (150 W)–950 kHz (300 W)	0.0564(1)
40 kHz (150 W)–200 kHz (300 W)	0.0691(3)
28 kHz (300 W)–200 kHz (300 W)	0.0564(1)
28 kHz (300 W)–950 kHz (300 W)	0.0554(2)

for an improvement of capacity maintenance. It is also indicated that a higher power in a supersonic-wave treatment is favorable in order to realize better cathode performance.

3.3. Characterization after a charge–discharge cycle test

After the charge–discharge cycle tests, we investigated crystal structures of the cathodes with XRD and Mn dissolution amounts into the electrolytes with ICP. Fig. 8 shows the XRD patterns and Table 5 lists the ratios of the FWHM of the diffraction peak (1 1 1) after the cycle tests to that before the cycle tests. While the FWHM of $LiMn_2O_4$ before the treatments became twice after the cycle tests, the changes in the FWHMs were insignificant for the samples exhibiting better cycle performances, i.e. after the step-by-step supersonic-wave treatments represented as "28 kHz (300 W)–200 kHz (300 W)" and "28 kHz (300 W)–950 kHz (300 W)". As shown in Table 6, Mn dissolution amounts of these samples were also suppressed compared with $LiMn_2O_4$. These results indicate that the step-by-step supersonic-wave treatments with the power as 300 W stabilize the crystal structure and thus keep them the spinel-type even during charge–discharge cycles. Similar tendencies were also reported in our previous work on $LiMn_{2-x}Zn_xO_4$ [17–19]. This effect of the treatments is considered to be important for a cycle performance improvement of the spinel-type $LiMn_2O_4$. Such a crystal structure stabilization was presumably due to a partial substitution of Zn for Mn and/or surface coating of Zn compounds resulting from the step-by-step supersonic-wave treatments.

3.4. Crystal structure analysis

In order to discuss an effect of the step-by-step supersonic-wave treatments on the crystal structure of $LiMn_2O_4$ in detail, we performed the Rietveld analysis using neutron diffraction patterns. Fig. 9 shows Rietveld refinement patterns of a sample after the step-by-step supersonic-wave treatment [28 kHz (150 W)–200 kHz (300 W)], and Table 7 listed the refined structure parameters and the *R*-values. As a preliminary analysis, we performed a refinement assuming a Zn compound like ZnO as a surface coating species, i.e. a secondary phase, but could not confirm its existence from the neutron diffraction pattern. Therefore, the refinement shown in Fig. 9 and Table 7 did not consider the existence of the surface coating species although site occupancies of Mn and Zn were optimized keeping their total value as unity. The calculated diffraction patterns were well fitted to the experimentally obtained ones as shown in Fig. 9, and the *R*- and *S*-values seemed sufficiently low. The analytical result indicates that about 1 mol% of Mn is substituted by Zn in the sample after the step-by-step supersonic-wave treatment. The occupancy of Zn was essentially lower than that expected from compositional analysis by ICP under the hypothesis that all of Zn can be substituted for Mn. Considering this, the residue of Zn might coat $LiMn_2O_4$ particles.

Table 7
Final results of Rietveld refinements for the sample after the step-by-step supersonic-wave treatment [28 kHz (150 W)–950 kHz (300 W)] at room temperature. *B* is an isotropic thermal parameter. Numbers in parentheses are estimated standard deviations of the last significant digit, and those without a deviation were fixed. *R*-factors were R_{wp} = 7.46%, R_p = 5.51%, R_e = 4.34% and S = 1.72. The refined lattice parameter was a = 0.82333(8) nm.

Atom	Site	x	y	z	$B/\times10^2$ nm^2	Site occupancy
Li	8a	0	0	0	1.6(4)	1
Mn	16d	5/8	5/8	5/8	0.1	0.992(5)
Zn	16d	=Mn(x)	=Mn(y)	=Mn(z)	=Mn(B)	$=1-g$(Mn)
O	32e	0.3878(2)	=x	=x	1.16(7)	1

$LiMn_{2-x}Zn_xO_4$: 85.5%; Al (from the apparatus): 14.5%

4. Conclusions

In order to improve cathode properties of $LiMn_2O_4$, we performed step-by-step supersonic-wave treatments on $LiMn_2O_4$ powder in a Zn-containing aqueous solution.

As for the samples after the step-by-step supersonic-wave treatments, we analyzed the crystal structure using X-ray and neutron diffractions and the metal composition using ICP and XPS. These analyses suggested that the treatment induced both a partial substitution of Zn for Mn and a surface coating by Zn compounds. Charge–discharge cycle tests revealed that the cathode property of

$LiMn_2O_4$ was drastically improved by the step-by-step supersonic-wave treatments, especially applying lower and higher frequencies as the first and second steps, respectively, with higher power. Such an improvement was considered to be due to the partial substitution and/or the surface modification. From the characterization of the cathodes and the electrolytes after the cycle tests, it was indicated that the crystal structures of the samples exhibiting better cycle performances were much stabilized.

Throughout this work, we demonstrated the step-by-step supersonic-wave treatments were effective for the cathode performance improvements even without any heat-treatments.

Acknowledgements

We were indebted to Dr. K. Ohoyama and Mr. K. Nemoto (Tohoku University) for assisting with the powder neutron diffraction measurements at HERMES (JRR-3M). This work was partly supported by MEXT, HAITEKU (2005–2007).

References

[1] D.H. Jang, Y.J. Shin, S.M. Oh, J. Electrochem. Soc. 143 (1996) 2204–2211.
[2] Y. Xia, Y. Zhou, M. Yoshio, J. Electrochem. Soc. 144 (1997) 2593–2600.
[3] Y. Idemoto, N. Koura, K. Udagawa, Electrochemistry 67 (1997) 235–237.
[4] M.M. Thackeray, Y. Shao-Horn, A.J. Kahaian, K.D. Kepler, E. Skinner, J.T. Vaughey, S.A. Hackney, Electrochem. Solid-State Lett. 1 (1998) 7–9.
[5] T. Inoue, M. Sano, J. Electrochem. Soc. 145 (1998) 3704–3707.
[6] Y. Shin, A. Manthiram, Electrochem. Solid-State Lett. 5 (2002) A55–A58.
[7] J.-S. Kim, J.T. Vaughey, C.S. Johnson, M.M. Thackeray, J. Electrochem. Soc. 150 (2003) A1498–A1502.
[8] R.J. Gummow, A. de Kock, M.M. Thackeray, Solid State Ionics 69 (1994) 59–67.
[9] L. Guohua, H. Ikuta, T. Uchida, M. Wakihara, J. Electrochem. Soc. 143 (1996) 178–182.
[10] K. Amine, H. Tukamoto, H. Yasuda, Y. Fujita, J. Electrochem. Soc. 143 (1996) 1607–1613.
[11] Q. Zhong, A. Bonakdarpour, M. Zhang, Y. Gao, J.R. Dahn, J. Electrochem. Soc. 144 (1997) 205–213.
[12] Y. Ein-Eli, W.F. Howard Jr., S.H. Lu, S. Mukerjee, J. McBreen, J.T. Vaughey, M.M. Thackeray, J. Electrochem. Soc. 145 (1998) 1238–1244.
[13] L. Hernán, J. Morales, L. Sánchez, J. Santos, Solid State Ionics 118 (1999) 179–185.
[14] Y. Idemoto, S. Ogawa, Y. Uemura, N. Koura, J. Ceram. Soc. Jpn. 108 (2000) 848–853.
[15] S.-T. Myung, S. Komaba, N. Kumagai, J. Electrochem. Soc. 148 (2001) A482–A489.
[16] Y. Idemoto, T. Ozasa, N. Koura, J. Ceram. Soc. Jpn. 109 (2001) 771–776.
[17] Y. Ito, Y. Idemoto, Y. Tsunoda, N. Koura, Electrochemistry 70 (2002) 847–849.
[18] Y. Ito, Y. Idemoto, Y. Tsunoda, N. Koura, J. Power Sources 119–121 (2003) 733–737.
[19] Y. Ito, Y. Idemoto, Y. Tsunoda, N. Koura, Electrochemistry 71 (2003) 703–709.
[20] Y. Idemoto, K. Horiko, Y. Ito, N. Koura, K. Ui, Electrochemistry 72 (2004) 680–687.
[21] G.G. Amatucci, A. Blyr, C. Sigala, P. Alfonse, J.M. Tarascon, Solid State Ionics 104 (1997) 13–25.
[22] S.-C. Park, Y.-S. Han, Y.-S. Kang, P.S. Lee, S. Ahn, H.-M. Lee, J.-Y. Lee, J. Electrochem. Soc. 148 (2001) A680–A686.
[23] A.M. Kannan, A. Manthiram, Electrochem. Solid-State Lett. 5 (2002) A167–A169.
[24] Y.-K. Sun, Y.-S. Lee, M. Yoshio, K. Amine, Electrochem. Solid-State Lett. 5 (2002) A99–A102.
[25] Z. Liu, H. Wang, L. Fang, J.Y. Lee, L.M. Gan, J. Power Sources 104 (2002) 101–107.
[26] J.-S. Kim, C.S. Johnson, J.T. Vaughey, S.A. Hackney, K.A. Walz, W.A. Zeltner, M.A. Anderson, M.M. Thackeray, J. Electrochem. Soc. 151 (2004) A1755–A1761.
[27] C. Li, H.P. Zhang, L.J. Fu, H. Liu, Y.P. Wu, E. Rahm, R. Holze, H.Q. Wu, Electrochim. Acta 51 (2006) 3872–3883.
[28] K.-N. Jung, S.-I. Pyun, Electrochim. Acta 52 (2007) 5453–5461.
[29] Y. Idemoto, N. Kitamura, H. Iwatsuki, Electrochemistry 76 (2008) 808–812.
[30] K. Ohoyama, T. Kanouchi, K. Nemoto, M. Ohashi, T. Kajitani, Y. Yamaguchi, Jpn. J. Appl. Phys. 37 (1998) 3319–3326.
[31] F. Izumi, T. Ikeda, Mater. Sci. Forum 321–324 (2000) 198–203.